HHS Public Access

Author manuscript

Retina. Author manuscript; available in PMC 2020 July 01.

Published in final edited form as:

Retina. 2019 July ; 39(7): 1333–1342. doi:10.1097/IAE.0000000000002156.

Comparison of retinal pathology visualization in multi-spectral scanning laser imaging

Amit Meshi, MD[1], **Tiezhu Lin, MD**[1,2], **Kunny Dans, MD**[1], **Kevin C. Chen, MD**[1], **Manuel Amador, MD**[1,3], **Kyle Hasenstab, PhD**[4], **Ilkay Kilic Muftuoglu, MD**[1,5], **Eric Nudleman, MD**[6], **Daniel Chao, MD**[6], **Dirk-Uwe Bartsch, PhD**[1], and **William R. Freeman, MD**[1]

[1]Department of Ophthalmology, Jacobs Retina Center at Shiley Eye Institute, University of California San Diego, La Jolla, California, USA

[2]He Eye Hospital, He University, Shenyang, China

[3]Escuela Superior de Oftalmologia, Instituto Barraquer de America, Bogota, Colombia

[4]Department of Ophthalmology, Hamilton Glaucoma Center at Shiley Eye Institute, University of California San Diego, La Jolla, California, USA

[5]Department of Ophthalmology, Istanbul Training and Research Hospital, Istanbul, Turkey

[6]Department of Ophthalmology, Shiley Eye Institute, University of California San Diego, La Jolla, California, USA

Abstract

Purpose—To compare retinal pathology visualization in multi-spectral scanning laser ophthalmoscope (MS SLO) imaging between the Spectralis and Optos devices.

Methods—This retrospective cross-sectional study included 42 eyes from 30 patients with age-related macular degeneration (AMD, 19 eyes), diabetic retinopathy (DR, 10 eyes) and epiretinal membrane (ERM, 13 eyes). All patients underwent retinal imaging with a color fundus camera (broad spectrum white light), the Spectralis HRA-2 system (3-color monochromatic lasers) and the Optos P200 system (2-color monochromatic lasers). The Optos image was cropped to a similar size as the Spectralis image. Seven masked graders marked retinal pathologies in each image within a 5 × 5 grid that included the macula.

Results—The average area with detected retinal pathology in all eyes was larger in the Spectralis images compared to Optos images (32.4% larger, $p < 0.0001$), mainly due to better visualization of ERM and retinal hemorrhage. The average detection rate of AMD and DR pathologies was similar across the 3 modalities, whereas ERM detection rate was significantly higher in the Spectralis images.

Corresponding author: William R. Freeman, MD, University of California at San Diego, Shiley Eye Institute, 0946, 9415 Campus Point Drive, La Jolla, CA 92037; Tel: (858) 534-3513; Fax: (858) 534-7985; wrfreeman@ucsd.edu.

DU Bartsch has received research support from Heidelberg Engineering. The other authors have no proprietary, financial, or conflicts of interest to disclose.

Conclusion—Spectralis tricolor MS SLO imaging had higher rate of pathology detection primarily due to better ERM and retinal hemorrhage visualization compared with Optos bicolor MS SLO imaging.

Keywords

Retinal imaging; scanning laser ophthalmoscope; multi-spectral imaging; multicolor imaging; retinal pathology visualization

Introduction

Color fundus photography (CFP) is a fundamental tool in ophthalmology which has been widely used in clinical practice for screening, documentation and follow up of retinal pathologies for many decades. The appearance on CFP closely resembles findings on clinical examination because of the broad-spectrum illumination used in fundus cameras. Numerous enhancements such as digital imaging, nonmydriatic functions and wide-field technology made CFP an essential component of ophthalmic examination.[1] However, CFP is limited by media opacities, limited resolution and contrast and patient inconvenience due to the bright white light illumination.[2]

The scanning laser ophthalmoscope (SLO) offers an alternative method of capturing fundus images since it was first introduced in 1980.[3] SLO devices use a single point of laser light at a specific wavelength to scan across the retina in a series of parallel horizontal lines. In this way, the effects of light scatter are reduced. Thus, images produced by the SLO have a higher contrast and resolution compared to standard fundus cameras.[1,4,5] The use of confocal aperture in SLO systems further improves image quality by allowing only light returning from a specific plane of interest to be used to reconstruct the fundal image.[4,6]

SLO fundus imaging is well suited to monochromatic image acquisition because it typically uses laser light sources at a number of fixed wavelengths.[1] Different wavelengths of light penetrate the retinal surface at different depths. Longer wavelengths of light penetrate more deeply and thus may enhance viewing of deep retinal and choroidal structures. Conversely, the use of shorter wavelengths of light allows improved imaging of superficial retinal structures.[7] Advanced SLO systems can use 2–4 different monochromatic laser light sources to capture several simultaneous reflectance images. A single multi-spectral (MS) image can be generated by merging the information of these reflectance images. The result is a color-like, high-resolution, high-contrast image that contains information from different retinal layers depending on the wavelength of laser used.

Multi-spectral SLO imaging was shown to be superior to CFP in detecting most early and late age-related macular degeneration (AMD) features,[8,9] demarcation of neurosensory detachment areas in central serous chorioretinopathy[2] and visualization of epiretinal membrane (ERM).[10] Multi-spectral imaging was also more detailed than CFP in the detection of acute macular neuroretinopathy.[11]

The Spectralis HRA-2 system (Heidelberg Engineering, Heidelberg, Germany) and the Optos P200 system (Optos, Dunfermline, Scotland) possess MS SLO imaging capability.

There are several differences between the two SLO devices. Firstly, the Spectralis system has a confocal aperture while the Optos system uses non-confocal optics. The confocal aperture limits depth of field and increases resolution in lateral and axial direction, whereas the non-confocal optics yields a large depth of field without the need for focus adjustment. Secondly, the field of view is substantially different between these devices. The Spectralis has 30°–55° external field of view, whereas the Optos has 135° external field of view (200° internal field of view).[12] Another important difference is the number and wavelengths of lasers used to generate the MS image. In the Spectralis, the MS image is created by using 3 monochromatic laser sources: blue (488 nm), green (515 nm) and infrared (820 nm). In the Optos, the MS image is created by combining only 2 monochromatic laser sources: green (532 nm) and red (635 nm).

Multi-spectral SLO imaging of the Spectralis and Optos has become widely popular and routinely used in clinical practice. In many instances, it replaces CFP in the evaluation and follow-up of retina patients because it is incorporated in a multimodal single device. However, the appearance of fundus structures and retinal pathologies on MS SLO images are different from CFP and clinical examination. For example, the Spectralis MS SLO image is generally more red-orange and the optic disc and blood vessels are much darker than what is observed on CFP. The Optos MS SLO image, on the other hand, has dominant green hue compared with CFP. Thus, it is of great interest to investigate the ability to detect retinal pathologies on MS SLO images given their different appearance compared with traditional CFP. In addition, we wanted to assess differences in retinal pathology visualization between these two devices.

Methods

This retrospective cross-sectional study was conducted according to the principles of the Helsinki Declaration. Institutional Review Board (IRB) approval was acquired from University of California, San Diego (UCSD) for the review and analysis of patient data (IRB number: 120516). The study complied with the Health Insurance Portability and Accountability Act of 1996.

Patients with AMD, diabetic retinopathy (DR) or ERM seen at the Shiley Eye Institute, UCSD between November 2016 and April 2017 were included in this study if they had CFP and MS SLO imaging with the Spectralis HRA-2 system and Optos P200 system. CFP and Spectralis MS SLO imaging are routinely obtained in all our patients as part of standard clinical care. Optos imaging is done in a subset of patients to view the retina periphery as well. Only patients who were imaged by all three modalities within a week and had good quality images were included. Patients' pupils were dilated with tropicamide 1% and phenylephrine 2.5% prior to all image capturing. Imaging with the Spectralis was performed as follows. After proper alignment of the patient's eye we turned on the infrared light source and adjusted pupil centration, eye-instrument distance and defocus until the retinal vessels appeared in highest contrast. Throughout our imaging session the operator continuously adjusted these three parameters to ensure proper image settings. Spectralis imaging was performed using the default high-speed mode and the automatic real-time (ART) mode, averaging a total of 15 single images. Imaging with the Optos was performed as follows.

The patient was placed at the instrument and the head rotation and instrument-eye distance was adjusted to ensure proper pupil centration. Images were recorded in a snap-shot with automatic focusing. CFP followed established retinal photography standards and was obtained using a fundus camera-based flash system (TRC-50DX, Topcon Medical Systems, Oakland, NJ) with 35° field of view. The field of view was 30° and 135° (200° internal field of view) for the Spectralis and Optos, respectively.

The anonymized, full-size images were exported from each camera: Topcon 3000 × 2672 pixels, Spectralis 768 × 768 pixels and Optos 3900 × 3072 pixels. The Optos image was cropped using Adobe Photoshop software (Adobe Systems Inc, San Jose, CA) to a similar size as the Spectralis image (768 × 768 pixels) to include the macula. Any image identifier (title, scale) was removed from all images with the Photoshop software using the spot healing brush tool. No other image alteration was made.

Seven retina specialists (T.L., K.D., M.A., K.C., I.K.M., E.N., D.C.) graded the images in 2 parts. In the first part, all images of all eyes were presented separately in a masked fashion and in a random order using Microsoft PowerPoint (Microsoft Corporation, Redmond, WA). Each grader viewed the slides on his/her own personal computer screen in a dim room with screen settings standardized to the highest available resolution. The graders were instructed to mark as many retinal pathologies as possible in a given image within a 5 × 5 square grid (6.5 mm by 6.5 mm) centered in the fovea (Figure 1). The grid size was designed to include the macula area and was adjusted for each modality to correct for magnification differences between them by an independent operator who was not a grader (D.U.B). All cells of the grid containing the same pathology were marked in a binary fashion. If more than one type of pathology were in a cell, each pathology was marked separately. For our analysis, we considered a pathology to be present in a given eye based on complete clinical evaluation (clinical diagnosis, clinical exam and imaging). The number of marked cells was counted for each pathology in every image for each grader. The average number of marked cells was calculated for all eyes, for each disease (AMD, DR, ERM) and for each retinal pathology. A pathology detection rate was defined as the percent of graders that identified the pathology on a given image, regardless of the number of marked cells. The average detection rate was calculated for each disease, retinal pathology and overall. Artifacts in the images were also noted in this part.

In the second part, the 3 images (Topcon, Spectralis and Optos) of each eye were grouped together in a masked fashion using Microsoft PowerPoint (Figure 2). The graders were instructed to rank the images according to the quality of retinal pathology visualization: from best visualization (1) to worst visualization (3).

Statistical analysis

Statistical analyses were performed using R (www.r-project.org). Intergrader and inter-modality agreement of the number of cells occupied by retinal lesions was assessed using the concordance correlation coefficient (CCC) for each disease and overall. The inter-modality agreement corresponds to the within-grader pairwise concordance of the number of marked cells between the three imaging modalities (intragrader agreement). The agreement was considered strong for coefficient value ranging from 0.70–0.89, moderate for coefficient

value ranging from 0.50–0.69 and weak for coefficient value ranging from 0.30–0.49.[13] Statistical differences in the number of cells between imaging modalities and differences in the detection rates of the imaging modalities were calculated using mixed-effects model contrasts for each disease, retinal pathology and overall. P-values of the differences were adjusted for multiple comparisons using the Tukey-Kramer method. Imaging modality was included as a fixed effect and an intercept nested within eye was included as a random effect to account for repeated measurements within eye. Rankings were analyzed by the percentage of images ranked first or second for each modality. Confidence intervals were placed on ranking rates using exact binomial testing.

Results

Forty-two eyes from 30 patients with AMD (19 eyes), DR (10 eyes) and ERM (13 eyes) were included in this study. Table 1 summarizes the differences in appearance of common retinal pathologies between the Topcon, Spectralis and Optos images. Figures 3, 4 and 5 show examples of AMD, DR and ERM lesions, respectively, as they appear on the three imaging modalities.

The overall intergrader agreement between the 7 retina specialists of the number of cells occupied by retinal lesions was moderate, but similar, across the three imaging modalities (Topcon: CCC = 0.64, 95% CI = 0.54, 0.73; Spectralis: CCC = 0.62, 95% CI = 0.53, 0.70; Optos: CCC = 0.59, 95% CI = 0.47, 0.68). The intergrader agreement for AMD, DR and ERM is shown in table 2. The overall inter-modality agreement (overall intragrader pairwise concordance) of the number of marked cells was strong between the Topcon and Optos images (CCC = 0.79, 95% CI = 0.74, 0.82) and moderate between the Topcon and Spectralis images (CCC = 0.65, 95% CI = 0.60, 0.70) and between the Spectralis and Optos images (CCC = 0.59, 95% CI = 0.53, 0.64). The inter-modality agreement for AMD, DR and ERM is shown in table 3.

The average number of marked cells with pathology in all eyes was significantly higher in Spectralis images (6.50 cells) compared with Topcon images (5.07 cells, $p < 0.0001$) and Optos images (4.91 cells, $p < 0.0001$). There was no significant difference in the average number of cells between the Topcon and Optos images ($p = 0.67$). The difference between the Spectralis and Topcon images was due to significantly more marked cells containing ERM (average difference (AD) 8.13 cells, $p < 0.0001$) and nonspecific RPE changes in AMD (AD 2.25 cells, $p = 0.0003$) in the Spectralis images. The difference between the Spectralis and Optos images was mainly influenced by significantly more marked cells containing ERM (AD 8.92 cells, $p < 0.0001$), microaneurysms (AD 2.64 cells, $p < 0.0001$) and retinal hemorrhage (AD 2.51 cells, $p < 0.0001$) in the Spectralis images. The average number of marked cells with choroidal nevus was significantly higher in Optos images compared with Spectralis images (AD 2.24 cells, $p = 0.015$). The average difference of marked cells for each retinal pathology between the three imaging modalities is presented in table 4.

Pathology detection rate was defined as the percent of graders that identified the pathology on a given image. The average detection rate of retinal pathologies in all eyes was not

different between the three imaging modalities (Topcon 0.65, Spectralis 0.66, Optos 0.66, all $p > 0.05$). The average detection rate of AMD and DR pathologies was similar across all modalities, but ERM detection rate was significantly higher in Spectralis images (0.92) compared with Topcon images (0.69, $p = 0.001$) and Optos images (0.68, $p = 0.0007$). Comparison of the average detection rate for each retinal pathology between the three imaging modalities is presented in table 5.

We compared the ranking of retinal pathology visualization quality between the three imaging modalities. Topcon images were ranked first or second 83% of the times (95% CI = 78%, 87%), Spectralis images 67% of the times (95% CI = 61%, 72%) and Optos images 50% of the times (95% CI = 44%, 56%). Topcon images received the highest ranking in AMD and DR eyes, whereas Spectralis images received the highest ranking in ERM eyes (Table 6).

The most common artifacts observed in SLO imaging were a white hyper-reflective artifact in the Spectralis images and a white “equal sign” artifact in the Optos images (Figure 5). There was no difference in the proportion of images with artifacts between the Optos (47.6% of images) and the Spectralis images (35.7% of images, $p = 0.38$).

Discussion

In this study, we compared retinal pathology visualization between MS SLO images of the Spectralis and the Optos devices. We found that overall larger area of macular involvement and better ERM detection were noted in the Spectralis images compared with the Optos images. The Spectralis images also received higher ranking for better ERM visualization quality than the Optos images. Nevertheless, the overall detection of retinal pathology was similar between them and CFP. These results suggest that both MS images of the Spectralis and Optos can be used reliably in clinical setting for the diagnosis and follow-up of common retinal conditions with better ERM detection and visualization in the Spectralis images.

More cells occupied by retinal lesions were seen overall in the Spectralis images compared with the Optos images. This difference was mainly derived by the significantly better visualization of ERM and retinal hemorrhage in the Spectralis images. Detection rate of ERM was also significantly higher in the Spectralis images than in the Optos images. Reznicek et al[14] previously compared ERM visualization between the Spectralis and Optos MS SLO images. Better ERM detectability and more accurate ERM marking were found in the MS image and in the green and blue reflectance images of the Spectralis than in the Optos images. We also recently showed that superior ERM detection and delineation of surface folds in the Spectralis image was primarily due to the green and blue channels.[10] Although the Optos uses a green light source for the MS image, it has a longer wavelength than the Spectralis and has no blue wavelength light source. Moreover, the confocal aperture of the Spectralis system, a feature that is absent in the Optos system, increases the axial and lateral resolution of the image. Improving the axial resolution results in better distinction of different planes, thus enhancing the perception of epiretinal structures. These differences in the optical design between the two devices make ERM more distinguishable in the Spectralis than the Optos MS image.

In our study, retinal hemorrhage and microaneurysms were better visualized in the Spectralis and color images compared to the Optos images, although with similar detection rates in all three of them. This may be the result of differences in image resolution, contrast and color balance between these modalities. Although the ultrawide field image of the Optos has a large number of pixels, cropping it to a 30° × 30° field-of-view decreases its pixilation compared to the Spectralis 30° field image. In our experience, the Spectralis images were more detailed and seemed to be sharper than the cropped Optos images. This difference might be explained by the different optical layout of the two instruments. However, when used in its full field-of-view, the Optos image was recently shown to have an excellent correlation of hemorrhage and microaneurysms counts to the standard Early Treatment Diabetic Retinopathy Study 7-field color photographs. In addition, almost 50% more lesions were identified in the peripheral fields of the ultrawide field images.[15] These findings suggest that cropping the Optos ultrawide field image may reduce its diagnostic capabilities and may not take full advantage of these images.

Despite the variability in the number of marked cells between the three imaging modalities, the detection rates of all retinal pathologies were similar between them, with the exception of ERM. These results reassure clinicians that it is possible to use MS SLO imaging for the assessment of retina patients, without the risk of missing common retinal pathologies. One should keep in mind that the color schemes used in the MS SLO images are different form the colors on CFP.[2] For example, pigmentary lesions appear as bright orange on the Spectralis, whereas retinal pigment epithelium atrophy appear as well demarcated gray-green area on the Optos. This is probably the reason we found lower choroidal nevus visualization in the Spectralis images compared to the color and Optos images. Therefore, the clinician should get familiar with MS SLO images and the way various retinal lesions appear on them before integrating these modalities in routine clinical use. In general, the Optos images have more natural colors that resemble CFP than the Spectralis images. This difference can be explained by the presence of an infrared imaging source in the Spectralis device. As a result, there was a strong overall inter-modality agreement between the Optos and Topcon grading, but only a moderate one between the Spectralis and Topcon. Nevertheless, the Spectralis images were ranked similarly to the Optos images for quality of retinal pathology visualization in AMD and DR and significantly higher in ERM. It is not surprising that our graders ranked the color images higher than the MS SLO images in most cases, but in ERM eyes. This is primarily influenced by the way clinicians are used to assess the retina clinically. Using the MS images on regular bases would improve the physician ability to diagnose retinal pathologies on these images while taking advantage of the higher contrast and resolution image compared to CFP. Another advantage of MS imaging over CFP is the ability to assess each laser channel individually to better identify the depth of the pathology.

Larger area of retinal involvement was noted on Spectralis images compared to color images in our AMD patients. In previous studies, many AMD features, such as drusen, reticular pseudodrusen, non-atrophy hypopigmentation, fibrosis and atrophy were detected more frequently on Spectralis images than on CFP.[8,9] In our study, nonspecific RPE changes were significantly better visualized with the Spectralis. Less light scatter on the MS SLO image and deeper penetration of infrared light enhance the viewing of the outer retinal layers and

choroid in the Spectralis images.[8,9,16,17] This difference may not be clinically significant due to the similar detection rates of AMD pathologies in our study, but better definition of AMD lesions on MS SLO imaging may improve automated detection of lesion margins and automated measurements of their dimensions in the future.

More than a third of the Spectralis images and almost half of the Optos images had some type of artifact. The most common artifacts were a white hyper-reflective artifact in the Spectralis images and a white "equal sign" artifact in the Optos images. Pang and Freund[18] previously described the hyper-reflective artifact in the Spectralis images and named it "ghost maculopathy". This artifact appears only in pseudophakic eyes and probably occurs because of reflection or scatter of near-infrared light from the posterior chamber intraocular lens. Recently, Feng et al[19] reported 3 additional types of artifacts observed in the Spectralis images: spot, wisp and net. These artifacts were detected in 37 of 159 of eyes (23.3%) in their study and were also lens-related. Besides the known eyelash artifacts in the Optos images,[20] we found high prevalence of white "equal sign" artifact. Despite the high frequency of artifacts in the MS SLO images, most artifacts were small, occupying only a little portion of the image, off-center and usually not blocking the view of the retina behind them. Clinicians should be aware of these artifacts for reliable interpretation of MS SLO images.

The overall intergrader agreement between the 7 graders was only moderate in our study. This might have created noise and caused large variability in our results. Nevertheless, the intergrader agreement was consistent in all three imaging modalities and we were able to show significant differences between them. Another possible weakness of our study may be related to the grid used for grading. Although the grid size was adjusted to correct for scale differences between the devices, its alignment did not perfectly match between them. This might have led to differences between the devices that were grid-related and not image-related. Our study may be also limited by the small sample size and by not analyzing each laser channel separately.

In conclusion, visualization of ERM and retinal hemorrhage was better in the Spectralis tricolor MS SLO imaging than in the Optos bicolor MS SLO imaging. The detection of AMD and DR features was similar between these modalities and CFP, but ERM detection was superior on the Spectralis. Thus, the clinician may use MS SLO imaging confidently instead of traditional CFP for the assessment of common retinal diseases after becoming familiar with the color variations and artifacts of this novel imaging technique.

Acknowledgments

Funding/Support: This study was supported in part by an NIH grant EY016323 (DUB) and an UCSD Vision Research Center Core Grant P30EY022589, an unrestricted fund from Research to Prevent Blindness, NY (WRF). The funding organization had no role in the design or conduct of this research.

References

1. Keane PA, Sadda SR. Retinal imaging in the twenty-first century: State of the art and future directions. Ophthalmology. 2014; 121:2489–2500. [PubMed: 25282252]

2. Tan ACS, Fleckenstein M, Schmitz-Valckenberg S, Holz FG. Clinical Application of Multicolor Imaging Technology. Ophthalmologica. 2016; 236:8–18. [PubMed: 27404384]
3. Webb RH, Hughes GW, Pomerantzeff O. Flying spot TV ophthalmoscope. Appl Opt. 1980; 19:2991–2997. [PubMed: 20234539]
4. Bartsch DU, Weinreb RN, Zinser G, Freeman WR. Confocal scanning infrared laser ophthalmoscopy for indocyanine green angiography. Am J Ophthalmol. 1995; 120:642–651. [PubMed: 7485366]
5. Freeman WR, Bartsch D, Mueller A, et al. Simultaneous indocyanine green and fluorescein angiography using a confocal scanning laser ophthalmoscope. Arch Ophthalmol. 1998; 116:455–463. [PubMed: 9565042]
6. Hassenstein A, Meyer CH. Clinical use and research applications of Heidelberg retinal angiography and spectral-domain optical coherence tomography - a review. Clin Exp Ophthalmol. 2009; 37:130–143. [PubMed: 19338610]
7. Spaide RF, Curcio CA. Drusen characterization with multimodal imaging. Retina. 2010; 30:1441–1454. [PubMed: 20924263]
8. Alten F, Clemens CR, Heiduschka P, Eter N. Characterisation of reticular pseudodrusen and their central target aspect in multi-spectral, confocal scanning laser ophthalmoscopy. Graefes Arch Clin Exp Ophthalmol. 2014; 252:715–721. [PubMed: 24276561]
9. Graham KW, Chakravarthy U, Hogg RE, et al. Identifying Features of Early and Late Age-Related Macular Degeneration: A Comparison of Multicolor Versus Traditional Color Fundus Photography. Retina.
10. Kilic Muftuoglu I, Bartsch DU, Barteselli G, et al. Visualization of Macular Pucker By Multicolor Scanning Laser Imaging. Retina.
11. De Salvo G, Vaz-Pereira S, Arora R, Lotery AJ. Multicolor imaging in the diagnosis and follow up of type 2 acute macular neuroretinopathy. Eye. 2017; 31:127–131. [PubMed: 27689963]
12. Espina M, Arcinue C, Ma F, et al. Analysis of a Confocal Scanning Laser Ophthalmoscope Noncontact Ultra-Wide Field Lens System in Retinal and Choroidal Disease. Retina. 2015; 35:2664–2668. [PubMed: 26584439]
13. Munk MR, Giannakaki-Zimmermann H, Berger L, et al. OCT-angiography: A qualitative and quantitative comparison of 4 OCT-A devices. PLoS One. 2017; 12:e0177059. [PubMed: 28489918]
14. Reznicek L, Dabov S, Kayat B, et al. Scanning laser “en face” retinal imaging of epiretinal membranes. Saudi J Ophthalmol. 2014; 28:134–138. [PubMed: 24843307]
15. Silva PS, El-Rami H, Barham R, et al. Hemorrhage and/or Microaneurysm Severity and Count in Ultrawide Field Images and Early Treatment Diabetic Retinopathy Study Photography. Ophthalmology. 2017; 124:970–976. [PubMed: 28336057]
16. Ben, Moussa N; Georges, A; Capuano, V; , et al. MultiColor imaging in the evaluation of geographic atrophy due to age-related macular degeneration. Br J Ophthalmol. 2015; 99:842–847. [PubMed: 25586715]
17. Badal J, Biarnés M, Monés J. Performance characteristics of multicolor versus blue light and infrared imaging in the identification of reticular pseudodrusen. Int Ophthalmol.
18. Pang CE, Freund KB. Ghost maculopathy: An artifact on near-infrared reflectance and multicolor imaging masquerading as chorioretinal pathology. Am J Ophthalmol. 2014; 158:171–178. e2. [PubMed: 24631479]
19. Feng HL, Sharma S, Stinnett S, et al. Characterization of Artifacts Associated With Multicolor Confocal Scanning Laser Ophthalmoscopy. Ophthalmic Surg Lasers Imaging Retina. 2017; 48:810–815. [PubMed: 29020424]
20. Inoue M, Yanagawa A, Yamane S, et al. Wide-Field Fundus Imaging Using the Optos Optomap and a Disposable Eyelid Speculum. JAMA Ophthalmol. 2013; 131:226. [PubMed: 23411888]

Summary statement

Compared to traditional color fundus photography, multi-spectral SLO imaging with either the Spectralis or the Optos devices can be used reliably in clinical setting for the diagnosis and follow-up of common retinal conditions with better epiretinal membrane detection and visualization in the Spectralis images.

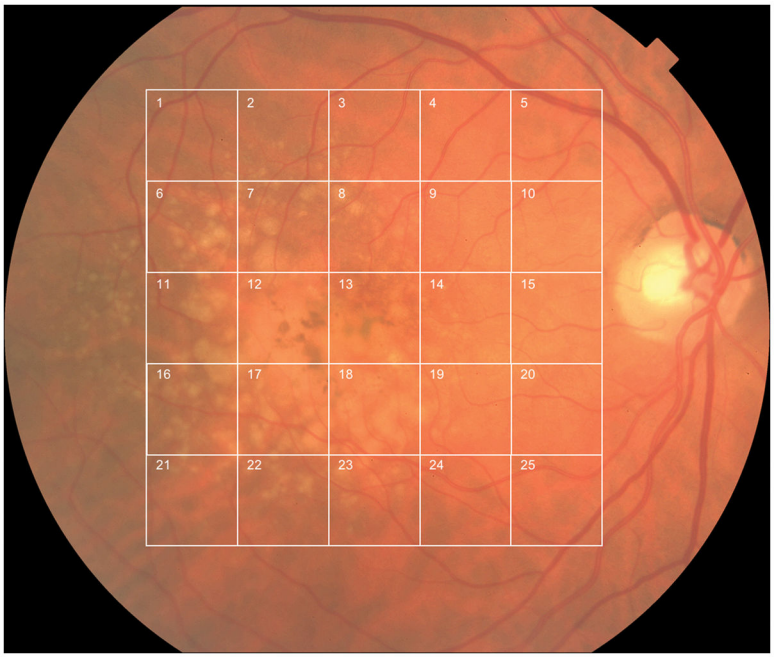

Figure 1.

A color fundus photo with a 5 × 5 square grid (6.5 mm by 6.5 mm) centered in the fovea. The graders were instructed to mark as many retinal pathologies as possible within the grid. The number of marked cells was counted for each pathology.

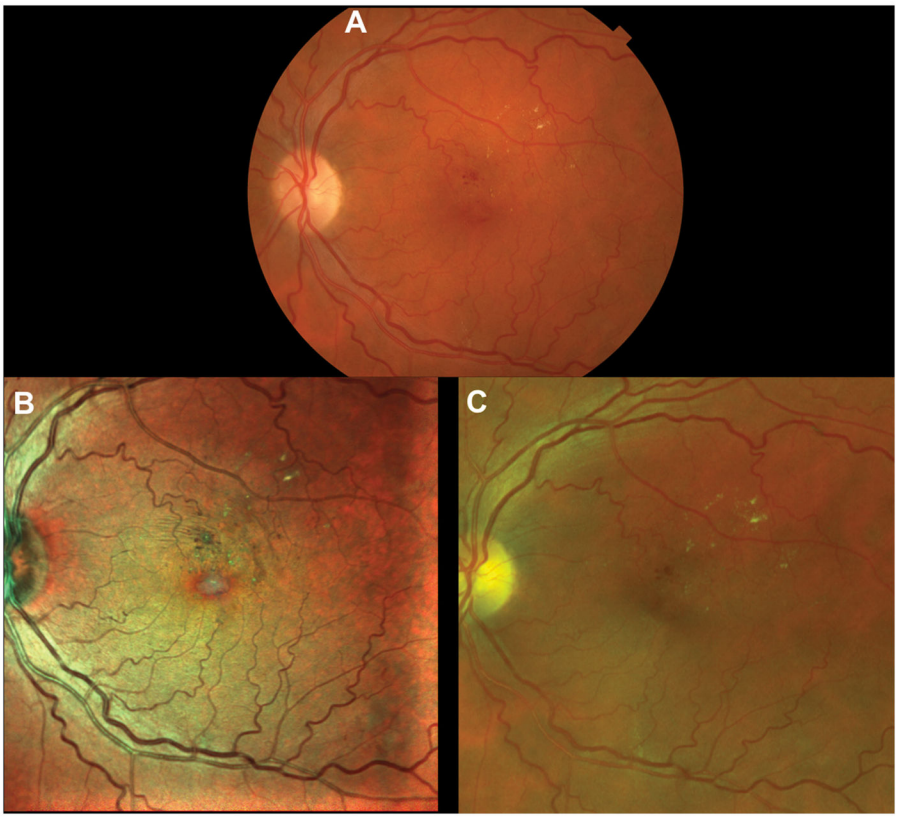

Figure 2.

(A) Topcon color fundus photo, (B) Spectralis multi-spectral scanning laser ophthalmoscope (MS SLO) image and (C) Optos MS SLO image of the same eye grouped together in a masked fashion for retinal pathology visualization quality ranking.

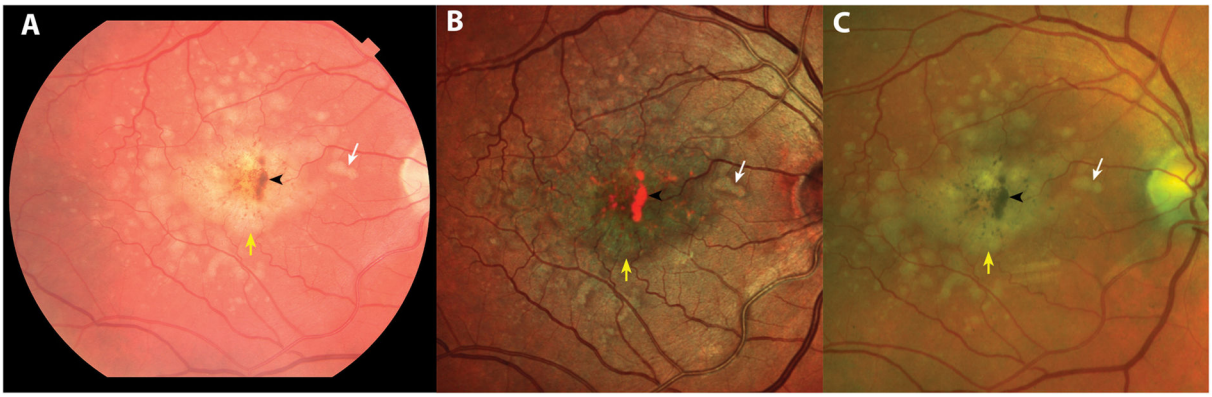

Figure 3.

Age-related macular degeneration lesions on (A) color fundus photography (CFP) image, (B) Spectralis multi-spectral scanning laser ophthalmoscope image (MS SLO) and (C) Optos MS SLO image. Drusen (white arrow) has yellow-green color and distinct borders on MS SLO images compared to the yellow color and fuzzy borders on the CFP image. Pigment epithelium detachment (yellow arrow) has a dark green color on the Spectralis image and yellow-green color on the Optos image compared to yellow color on the CFP image. Pigment clumps (black arrowhead) are bright orange on the Spectralis image compared to brown-black on the CFP and Optos images.

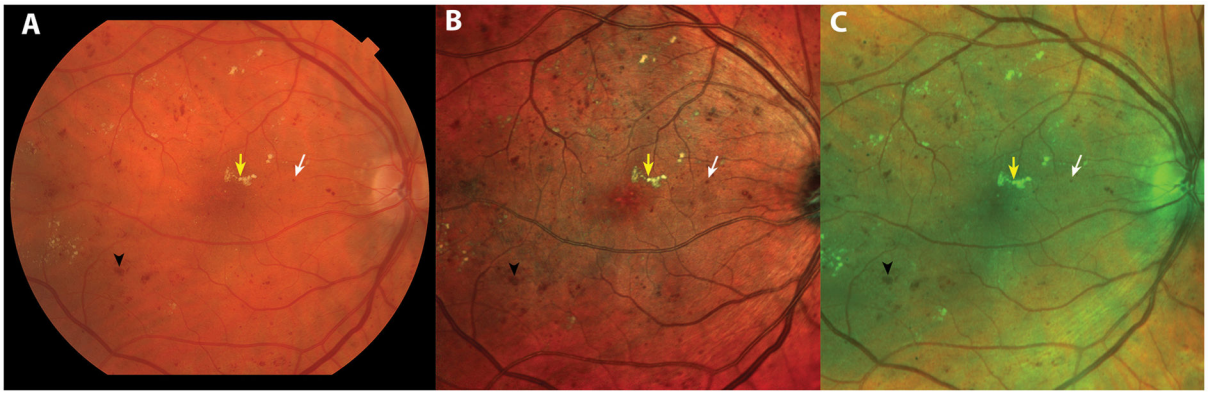

Figure 4.

Diabetic retinopathy lesions on (A) color fundus photography (CFP) image, (B) Spectralis multi-spectral scanning laser ophthalmoscope image (MS SLO) and (C) Optos MS SLO image. Microaneurysm (white arrow) and dot and blot hemorrhage (black arrowhead) are darker on the MS SLO images compared to the CFP image. Retinal hemorrhage is seen more clearly on the Spectralis than the Optos image. Hard exudates (yellow arrow) are yellow-green on the MS SLO images compared to yellow on the CFP image.

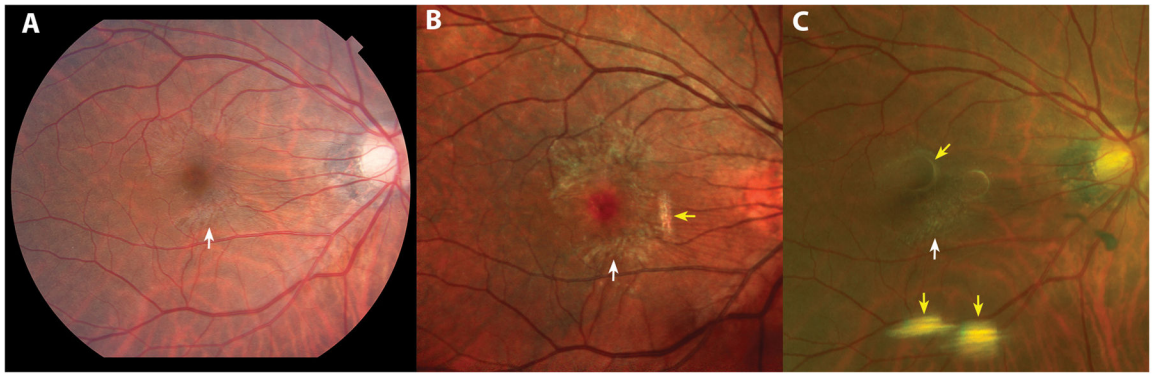

Figure 5.

Epiretinal membrane (ERM) (white arrow) on (A) color fundus photography (CFP) image, (B) Spectralis multi-spectral scanning laser ophthalmoscope image (MS SLO) and (C) Optos MS SLO image. The ERM is visible more clearly on the Spectralis image than on the CFP or Optos images. Artifacts (yellow arrows) are seen on both the Spectralis (hyper-reflective artifact) and the Optos (“equal sign” and ring artifacts) images.

Table 1

Appearance of common retinal pathologies in the Topcon, Spectralis and Optos images.

	Topcon	Spectralis	Optos
Drusen (Figure 3)	Round, yellowish deep lesions, fuzzy borders	Round, yellow-green deep lesions, distinct borders	Round, yellowish deep lesions, distinct borders
PED (Figure 3)	Deep elevated yellowish lesions, fuzzy borders	Deep elevated dark green lesions, fuzzy borders	Deep elevated yellow-green lesions, fuzzy borders
Pigment clumps (Figure 3)	Dark brown-black spots	Bright-orange spots	Dark brown-black spots
RPE atrophy	Yellow-white areas, sharp margins	Pale orange areas, sharp margins	Gray-green areas, sharp margins
RPE changes	Deep hypo- and hyper-pigmentation mottling	Deep red and brown mottling	Deep hypo- and hyper-pigmentation mottling
Microaneurysms (Figure 4)	Small red pinpoint dots	Small dark red pinpoint dots	Small red pinpoint dots
D/B hemorrhage (Figure 4)	Red spots	Dark red spots	Red-brown spots
Hard exudates (Figure 4)	Superficial yellow spots, distinct borders	Superficial yellow-green spots, distinct borders	Superficial yellow-green spots, distinct borders
ERM	Fine white-gray superficial sheath, striae	White-yellowish superficial sheath, striae	Fine white-yellowish superficial sheath, striae
Choroidal nevus	Deep brown lesion	Deep orange lesion	Deep dark green-brown lesion

PED = pigment epithelium detachment, RPE = retinal pigment epithelium, D/B = dot and blot, ERM = epiretinal membrane.

Table 2

Intergrader agreement of the number of cells occupied by retinal lesions in the Topcon, Spectralis and Optos images.

Disease	Modality	CCC	95% CI
Overall	Topcon	0.64†	0.54, 0.73
	Spectralis	0.62†	0.53, 0.70
	Optos	0.59†	0.47, 0.68
AMD	Topcon	0.71‡	0.50, 0.83
	Spectralis	0.41*	0.28, 0.54
	Optos	0.60†	0.44, 0.71
DR	Topcon	0.60†	0.43, 0.74
	Spectralis	0.54†	0.38, 0.68
	Optos	0.62†	0.38, 0.78
ERM	Topcon	0.50†	0.30, 0.66
	Spectralis	0.81‡	0.64, 0.90
	Optos	0.42*	0.25, 0.60

*Weak agreement (0.30–0.49)

†Moderate agreement (0.5–0.69)

‡Strong agreement (0.70–0.89)

CCC = concordance correlation coefficient, CI = confidence interval, AMD = age-related macular degeneration, DR = diabetic retinopathy, ERM = epiretinal membrane.

Table 3

Inter-modality agreement of the number of cells occupied by retinal lesions between the Topcon, Spectralis and Optos images.

Disease	Modality pairs	CCC	95% CI
Overall	Topcon-Spectralis	0.65†	0.60, 0.70
	Topcon-Optos	0.79≠	0.74, 0.82
	Spectralis-Optos	0.59†	0.53, 0.64
AMD	Topcon-Spectralis	0.54†	0.43, 0.64
	Topcon-Optos	0.78≠	0.72, 0.84
	Spectralis-Optos	0.58†	0.47, 0.67
DR	Topcon-Spectralis	0.83≠	0.77, 0.88
	Topcon-Optos	0.85≠	0.80, 0.89
	Spectralis-Optos	0.73≠	0.65, 0.80
ERM	Topcon-Spectralis	0.50†	0.41, 0.60
	Topcon-Optos	0.61†	0.45, 0.73
	Spectralis-Optos	0.39*	0.29, 0.49

*Weak agreement (0.30–0.49)

†Moderate agreement (0.5–0.69)

≠Strong agreement (0.70–0.89)

CCC = concordance correlation coefficient, CI = confidence interval, AMD = age-related macular degeneration, DR = diabetic retinopathy, ERM = epiretinal membrane.

Table 4

Average difference of marked cells between the Topcon, Spectralis and Optos images.

Disease/retinal pathology	Modality pairs	Average cell difference, n ± SE	P value
Overall	Topcon-Spectralis	−1.43 ± 0.19	< **0.0001**
	Topcon-Optos	0.16 ± 0.19	0.67
	Spectralis-Optos	1.59 ± 0.19	< **0.0001**
AMD	Topcon-Spectralis	−0.83 ± 0.25	**0.003**
	Topcon-Optos	−0.52 ± 0.25	0.10
	Spectralis-Optos	0.31 ± 0.25	0.43
Drusen	Topcon-Spectralis	0.10 ± 0.51	0.98
	Topcon-Optos	0.54 ± 0.51	0.54
	Spectralis-Optos	0.44 ± 0.51	0.66
PED	Topcon-Spectralis	−0.87 ± 0.51	0.20
	Topcon-Optos	−0.80 ± 0.51	0.26
	Spectralis-Optos	0.07 ± 0.51	0.99
Pigment clumps	Topcon-Spectralis	−0.93 ± 0.49	0.14
	Topcon-Optos	−1.52 ± 0.49	**0.007**
	Spectralis-Optos	−0.59 ± 0.49	0.45
RPE atrophy	Topcon-Spectralis	0.33 ± 0.54	0.82
	Topcon-Optos	0.04 ± 0.54	0.99
	Spectralis-Optos	−0.29 ± 0.54	0.86
RPE changes	Topcon-Spectralis	−2.25 ± 0.56	**0.0003**
	Topcon-Optos	−1.18 ± 0.56	0.09
	Spectralis-Optos	1.07 ± 0.56	0.14
DR	Topcon-Spectralis	−0.37 ± 0.29	0.42
	Topcon-Optos	0.72 ± 0.29	**0.038**
	Spectralis-Optos	1.08 ± 0.29	**0.0007**
Microaneurysms	Topcon-Spectralis	−0.49 ± 0.61	0.71
	Topcon-Optos	2.16 ± 0.61	**0.001**
	Spectralis-Optos	2.64 ± 0.61	< **0.0001**
D/B hemorrhage	Topcon-Spectralis	−0.35 ± 0.53	0.79
	Topcon-Optos	2.16 ± 0.53	**0.0002**
	Spectralis-Optos	2.51 ± 0.53	< **0.0001**
Hard exudates	Topcon-Spectralis	−0.31 ± 0.42	0.74
	Topcon-Optos	−1.00 ± 0.42	0.05
	Spectralis-Optos	−0.69 ± 0.42	0.23
Macular Edema	Topcon-Spectralis	0.70 ± 0.41	0.21
	Topcon-Optos	−0.27 ± 0.41	0.79
	Spectralis-Optos	−0.96 ± 0.41	0.05
ERM	Topcon-Spectralis	−8.13 ± 0.52	<**0.0001**

Disease/retinal pathology	Modality pairs	Average cell difference, n ± SE	P value
	Topcon-Optos	0.79 ± 0.52	0.29
	Spectralis-Optos	8.92 ± 0.52	**<0.0001**
Choroidal nevus	Topcon-Spectralis	1.52 ± 0.77	0.13
	Topcon-Optos	−0.71 ± 0.77	0.63
	Spectralis-Optos	−2.24 ± 0.77	**0.015**

Note: P-values of the differences were adjusted for multiple comparisons using the Tukey-Kramer method.

SE = standard error, AMD = age-related macular degeneration, PED = pigment epithelium detachment, RPE = retinal pigment epithelium, DR = diabetic retinopathy, D/B = dot and blot, ERM = epiretinal membrane.

Table 5

Comparison of the average detection rate of retinal pathologies between the Topcon, Spectralis and Optos images.

Disease/retinal pathology	Topcon detection rate ± SE	Spectralis detection rate ± SE	Optos detection rate ± SE	Topcon-Spectralis P value	Topcon-Optos P value	Spectralis-Optos P value
Overall	0.65 ± 0.03	0.66 ± 0.03	0.66 ± 0.03	0.92	0.93	0.99
AMD	0.62 ± 0.05	0.65 ± 0.05	0.66 ± 0.05	0.53	0.34	0.94
Drusen	0.82 ± 0.07	0.80 ± 0.07	0.81 ± 0.07	0.93	0.96	0.99
PED	0.32 ± 0.06	0.36 ± 0.06	0.39 ± 0.06	0.84	0.60	0.91
Pigment clumps	0.79 ± 0.09	0.80 ± 0.09	0.93 ± 0.09	0.99	0.37	0.45
RPE atrophy	0.78 ± 0.12	0.69 ± 0.12	0.76 ± 0.12	0.40	0.94	0.58
RPE changes	0.59 ± 0.11	0.80 ± 0.11	0.64 ± 0.11	**0.03**	0.73	0.10
DR	0.65 ± 0.05	0.61 ± 0.05	0.63 ± 0.05	0.48	0.80	0.86
Microaneurysms	0.71 ± 0.07	0.61 ± 0.07	0.57 ± 0.07	0.40	0.17	0.83
D/B hemorrhage	0.87 ± 0.06	0.87 ± 0.06	0.86 ± 0.06	1.0	0.84	0.84
Hard exudates	0.87 ± 0.07	0.84 ± 0.07	0.91 ± 0.07	0.87	0.77	0.47
Macular Edema	0.18 ± 0.04	0.05 ± 0.04	0.14 ± 0.04	0.07	0.79	0.23
ERM	0.69 ± 0.08	0.92 ± 0.08	0.68 ± 0.08	**0.001**	0.99	**0.0007**
Choroidal nevus	0.47 ± 0.11	0.14 ± 0.11	0.52 ± 0.11	0.19	0.94	0.13

Note: P-values of the differences were adjusted for multiple comparisons using the Tukey-Kramer method.

SE = standard error, AMD = age-related macular degeneration, PED = pigment epithelium detachment, RPE = retinal pigment epithelium, DR = diabetic retinopathy, D/B = dot and blot, ERM = epiretinal membrane.

Table 6

Proportion of 1st or 2nd ranking of the Topcon, Spectralis and Optos images according to retinal pathology visualization quality.

Disease	Modality	Proportion of 1st or 2nd ranking	95% CI
Overall	Topcon	0.83	0.78, 0.87
	Spectralis	0.67	0.61, 0.72
	Optos	0.50	0.44, 0.56
AMD	Topcon	0.81	0.74, 0.87
	Spectralis	0.57	0.48, 0.66
	Optos	0.62	0.53, 0.70
DR	Topcon	0.94	0.86, 0.98
	Spectralis	0.45	0.32, 0.57
	Optos	0.61	0.49, 0.73
ERM	Topcon	0.77	0.67, 0.85
	Spectralis	0.98	0.92, 1.00
	Optos	0.25	0.17, 0.35

CI = confidence interval, AMD = age-related macular degeneration, DR = diabetic retinopathy, ERM = epiretinal membrane.